Functional redundancy between UTY and UTX in regulating the localization of transcription factors involved in pluripotency

Tomohiko Akiyama[1,2,5], Toshiya Nakahara[2], Saeko Sato[2], Kei-ichiro Ishiguro[3], Masashi Yukawa[4], Miu Yamamoto[1], Hidehisa Takahashi[1], Minoru S H Ko[2]

1. Department of Molecular Biology, Yokohama City University, School of Medicine, Kanagawa 236-0027, Japan
2. Department of Systems Medicine, Keio University School of Medicine, Tokyo 160-8582, Japan
3. Department of Chromosome Biology, Institute of Molecular Embryology and Genetics (IMEG), Kumamoto University, Kumamoto 860-0811, Japan
4. Integrated Medical and Agricultural School of Public Health, Ehime University, Ehime 791-0295, Japan
5. Correspondence. akiyama.tom.pd@yokohama-cu.ac.jp

Abstract

The Y chromosome harbors few protein-coding genes, and their roles in early human development remain largely unclear. Here, we demonstrate that UTY, a Y-linked homolog of the histone demethylase UTX, plays a critical, demethylase-independent role in maintaining pluripotency in human embryonic stem cells (hESCs). Despite its low expression and weak enzymatic activity, UTY co-occupies active cis-regulatory elements with UTX and promotes the transcription of key pluripotency genes, including *NODAL* and *LEFTY*. Integrated genomic analyses of single and double knockout hESCs reveal that UTY and UTX function redundantly to maintain chromatin accessibility and ensure proper recruitment of core transcription factors such as OCT4 and SOX2. The combined loss of UTY and UTX disrupts transcription factor localization, induces widespread gene expression changes, and leads to a collapse of the pluripotent state, without detectable changes in H3K27 methylation. Instead, these defects are associated with impaired recruitment of ATP-dependent chromatin remodelers and reduced histone acetylation, suggesting a demethylase-independent mechanism. Our findings uncover an essential role for the evolutionarily conserved UTY in safeguarding enhancer function and transcription factor occupancy, highlighting Y-linked regulatory mechanisms that are critical for maintaining human pluripotency.

Introduction

The human X and Y chromosomes have evolved from a pair of ancestral autosomes (Lahn and Page 1999). While the X chromosome retains ~98% of the original gene content, the Y chromosome has undergone substantial degeneration and preserved only ~3% of ancestral genes (Skaletsky et al. 2003; Bellott et al. 2010; Mueller et al. 2013). Nevertheless, a select subset of Y-linked protein-coding genes has been evolutionarily conserved for at least 25 million years (Hughes et al. 2005; Hughes et al. 2012; Bellott et al. 2014). These genes encode proteins involved in key processes such as transcription, translation, and protein stability (Bellott et al. 2014; Hughes and Page 2015), and many are broadly expressed across somatic tissues (Godfrey et al. 2020), suggesting roles beyond male reproduction. However, their precise biological functions remain poorly defined. Understanding their contributions to development and aging may offer valuable insights into the evolutionary significance of the Y chromosome's gene repertoire.

Among these conserved Y-linked genes, UTY (Ubiquitously Transcribed Tetratricopeptide Repeat Gene on the Y chromosome) is of particular interest for its putative role in transcriptional regulation during early development, as supported by several lines of evidence.

UTY encodes a Jumonji C (JmjC) domain–containing protein, classified as a member of histone demethylase family (Klose et al. 2006). In vitro assays have indicated that UTY can demethylate trimethylated lysine 27 on histone H3 (H3K27), a repressive histone modification associated with gene silencing (Walport et al. 2014). However, UTY's enzymatic activity is substantially reduced relative to its X-linked homolog UTX (KDM6A) and no demethylase activity has been detected in cultured cells (Agger et al. 2007; Hong et al. 2007). By contrast, UTX has been characterized as a bona fide H3K27 demethylase required for lineage specification and differentiation (Seenundun et al. 2010; Lee et al. 2012; Mansour et al. 2012; Lei and Jiao 2018; Tang et al. 2020). Despite its limited catalytic activity, UTY is broadly expressed and has been conserved across mammals, raising the possibility that it fulfills a distinct, non-enzymatic regulatory role.

One potential role of UTY is to balance sex chromosome gene dosage between males and females. In preimplantation female embryos, both X chromosomes are transcriptionally active, resulting in elevated expression of X-linked genes relative to XY males. To restore dosage

equilibrium, X-inactivation is initiated around the time of implantation, leading to the stable transcriptional silencing of one X chromosome. However, UTX escapes X-inactivation (Greenfield et al. 1998) and is expressed from both alleles in females throughout development, while males rely on the combined expression of UTX and UTY. Given UTY's weak catalytic capacity, it remains unclear to what extent this co-expression provides functional compensation. Notably, Kabuki syndrome, a disorder caused by UTX haploinsufficiency and typified by growth delay and intellectual disability, is significantly more severe in males (UTX^–/Y) than in heterozygous females (UTX^+/–) (Lederer et al. 2014; Banka et al. 2015), indicating that UTY cannot fully substitute for UTX's enzymatic function during late stages of development.

By contrast, UTY appears to play a more effective compensatory role during early embryogenesis. In mouse models, deletion of UTX leads to embryonic lethality in homozygous females by E11.5, whereas hemizygous UTX-null males—which retain UTY—survive to term, albeit with reduced body size (Shpargel et al. 2012; Wang et al. 2012; Welstead et al. 2012). These sexually dimorphic phenotypes suggest that UTY and UTX act redundantly during early development, and that UTY's presence is sufficient to support embryogenesis in the absence of UTX. Consistent with this, catalytic activity of UTX is dispensable for early lineage commitment, including in neural precursor and mesodermal differentiation (Wang et al. 2012; Shan et al. 2020). Together, these indicate that UTY plays a critical, demethylase-independent role in early embryonic development.

This compensation may involve shared non-catalytic functions between UTX and UTY. UTX localizes to enhancers and promotes gene expression not only via H3K27 demethylation but also by recruiting coactivators such as p300 and the MLL3/4 methyltransferase complex (Wang et al. 2017). UTX also interacts with the BRG1-containing SWI/SNF chromatin remodeling complex to increase chromatin accessibility (Gozdecka et al. 2018) and forms nuclear condensates that facilitate MLL3/4 activity and long-range chromatin interactions (Shi et al. 2021). Although UTY lacks substantial catalytic activity, it may retain some of these non-enzymatic functions. Indeed, UTY has been proposed to share similar molecular partners with UTX, related to components of the H3K4 methylation COMPASS-like complex (Gazova et al. 2019). These shared non-catalytic activities may underlie the functional redundancy between UTX and UTY during early embryogenesis, yet the precise contributions of UTY to chromatin regulation remain poorly defined.

In this study, we revisit the role of UTY using human embryonic stem (ES) cells, which model early developmental gene regulatory networks and represent a stage when X-inactivation is being established. Using male ES cells, which harbor one allele each of UTX and UTY, we dissect their individual and combined contributions to maintaining pluripotency. Through analysis of UTX and UTY single- and double-knockout lines, we demonstrate that UTY supports enhancer activation, transcription factor occupancy, and the maintenance of an open chromatin state associated with pluripotency in the absence of UTX. These findings reveal that UTY plays a critical, non-catalytic role in sustaining transcriptional networks during early human development, functionally paralleling UTX.

Results

UTY Is Weakly Expressed Relative to UTX in Human Pluripotent Stem Cells

Although UTY exhibits lower demethylase activity compared to UTX, the two proteins share highly similar structures (Fig. 1A). UTY is broadly expressed across various human cells and tissues, but its expression levels in pluripotent stem cells—particularly in comparison to UTX—have not been well characterized. To address this, we analyzed publicly available RNA-sequencing data from five pluripotent stem cell lines (male), including three ES cell lines (SEES3 (Nakatake et al. 2020), H1 (Wei et al. 2021), WIBR1 (Theunissen et al. 2016)) and two iPS cell lines (585A1, NPC1.1 (Theunissen et al. 2016)). We quantified the expression levels of UTX and UTY using normalized transcript counts (TPM: transcripts per kilobase million). UTY expression was consistently low but detectable (approximately 2–12 TPM) across all lines, while UTX was expressed at 3- to 4-fold higher levels (approximately 7–48 TPM) (Fig. 1B). These results indicate that although UTY is transcribed in human pluripotent stem cells, its expression is markedly lower than that of UTX.

To directly compare UTX and UTY protein levels under identical conditions, we generated human ES cell lines in which a 3×Flag-HA epitope tag was inserted at the C-terminus of the endogenous *UTX* or *UTY* loci using CRISPR-Cas9 genome editing (Fig. 1C,D, and Supplemental Fig. S1). These knock-in cell lines, referred to as UTX-KI and UTY-KI, were derived from the SEES3 cell line, which exhibits the highest transcript levels among those examined. Immunoblotting with an HA antibody in these cell lines revealed that UTY protein levels were significantly lower than those of UTX (FC = 0.37) (Fig. 1E). Similarly,

immunostaining with a Flag antibody confirmed the reduced levels of UTY compared to UTX (FC = 0.66) (Fig. 1F). Expression of the pluripotency marker OCT4 was comparable between UTX-KI and UTY-KI cells.

These results demonstrate that although UTY is expressed in human ES cells, its protein levels are substantially lower than those of UTX. We hypothesized that this difference might arise from transcriptional regulation. However, comparative analysis of RNA polymerase II occupancy, H3K27 acetylation, and chromatin accessibility at the *UTX* and *UTY* promoters showed no significant differences (Fig. 1G). This suggests that the reduced expression of UTY is unlikely to be due to differences in transcriptional activation, and may instead result from lower RNA stability, shorter protein half-life, or other epigenetic mechanisms.

UTY is Co-localized with UTX at Promoters and Enhancers

To investigate the potential role of the weakly expressed UTY alongside UTX, we examined the genome-wide binding profiles of both proteins. We performed chromatin immunoprecipitation followed by sequencing (ChIP-seq) using an anti-Flag antibody in UTX-KI and UTY-KI cell lines. During optimization of the experimental conditions, we found that formaldehyde crosslinking alone was insufficient to capture ChIP-seq peaks, likely because UTX and UTY do not bind DNA directly. To overcome this, we used a dual crosslinking method with disuccinimidyl glutarate prior to formaldehyde fixation, which enhances the crosslinking of protein-DNA complexes (Tian et al. 2012). This approach improved data quality, yielding distinct and reproducible peaks for both proteins (Fig. 2A). Consistent with their expression levels, we identified ~37,000 UTX peaks and ~10,000 UTY peaks across biological triplicates (Fig. 2B). Despite this difference in peak number, both proteins showed similar genomic distributions: they were enriched at core promoters (0–0.5 kb), proximal regulatory regions (0.5–1 kb), and distal regulatory elements within ~50 kb of transcription start sites (TSS), likely corresponding to enhancers (Fig. 2B).

UTX and UTY binding regions substantially overlapped, with ~80% of UTY peaks co-localizing with UTX peaks (Fig. 2C), which we refer to as "both sites." Comparative analysis revealed a greater number of UTX-specific peaks. However, UTY signals were still detectable at most of these sites, although they did not exceed the peak-calling threshold (Fig. 2D); we designated these as "UTX-enriched sites." This indicates that most UTX-bound regions are also

occupied by UTY at lower levels. In contrast, only a small subset of UTY peaks showed minimal or no UTX signal and were defined as "UTY-enriched sites" (Fig. 2C,D). Together, these results suggest that UTY primarily functions in concert with UTX in human ES cells.

The co-localization of UTX and UTY was also observed in differentiated cells (endoderm cells derived from ES cells after 5 days of induction) (Fig. 2E). Most UTY signals overlapped with UTX, and low levels of UTY were detected at many UTX-enriched sites, whereas UTY-enriched sites were relatively few. These results indicate that UTX and UTY generally co-occupy similar genomic regions even in differentiated cells. Notably, the difference in binding levels between UTX and UTY—denoted as Δ(UTX−UTY)—was more pronounced in differentiated cells than in undifferentiated ES cells (Fig. 2F), suggesting that their functional divergence may emerge during differentiation.

To investigate the functional relevance of UTX and UTY co-occupancy in human ES cells, we analyzed gene expression associated with promoter-bound peaks. Most genes with promoter binding were actively transcribed, and those bound by both UTX and UTY exhibited higher transcriptional activity than those bound by UTX alone (Fig. 2G). These results suggest that UTX–UTY co-occupancy may enhance transcriptional activation. We performed similar analyses for UTY-enriched sites, but their low number and weak signal intensity limited the ability to draw definitive conclusions.

We further examined gene expression associated with distal UTX/UTY binding sites. Genes were grouped into three categories: those with binding exclusively at promoters, exclusively at distal regions (putative enhancers), and at both promoters and enhancers (Fig. 2H). Genes with both promoter and enhancer binding showed the highest expression levels (Fig. 2I). In contrast, genes with binding sites restricted to enhancers displayed both active and inactive states. A similar trend was observed for genes associated with UTX-enriched sites, although their expression levels were generally lower than those linked to co-bound regions (Fig. 2I,J). These results suggest that UTX–UTY co-occupancy promotes more robust and defined transcriptional regulation.

In differentiated cells, UTX and UTY were also detected at both promoters and distal regions (Supplemental Fig. S2A,B). These binding patterns were distinct from those of JMJD3, another

H3K27 demethylase that functions during ES cell differentiation (Burgold et al. 2008; Kartikasari et al. 2013; Akiyama et al. 2016). JMJD3 showed broad distribution from promoters to gene bodies, consistent with its catalytic role in H3K27 demethylation (Supplemental Fig. S2C,D), whereas UTX and UTY exhibited more discrete binding patterns. This aligns with previous findings showing that forced expression of JMJD3 alters H3K27 methylation in human ES cells, while UTX overexpression does not (Akiyama et al. 2016). These results suggest that the genomic localization of UTX and UTY reflects non-catalytic functions rather than enzymatic activity.

Identification of Genes Cooperatively Regulated by UTX and UTY

To further assess the functional redundancy of UTX and UTY, we generated human ES cell lines with single (UTX-KO and UTY-KO) and double (DKO) deletions using CRISPR-Cas9. Gene-specific deletions and homozygous mutations were confirmed in single and double knockout lines, respectively (Supplemental Fig. S3).

We performed RNA sequencing (RNA-seq) on these cell lines to evaluate transcriptomic changes. Genes located within 20 kb of UTX and/or UTY binding sites were analyzed and grouped according to their binding patterns: UTX-enriched, UTY-enriched, or co-occupied ("both-enriched"). Under single KO conditions, only a small subset of genes was differentially expressed, whereas DKO cells showed a markedly larger number of changes (Fig. 3A,B), with downregulation more frequent—supporting a role for UTX and UTY in transcriptional activation.

Furthermore, many genes with altered expression in DKO cells were shared among the three binding groups (Fig. 3C), suggesting cooperative regulation by UTX and UTY. Supporting this, UTX- and UTY-enriched sites were frequently located in close proximity, with a large proportion within 5 kb of each other (Fig. 3D). These findings indicate that UTX and UTY often co-occupy the same or adjacent genomic regions, enabling coordinated transcriptional regulation.

Gene ontology analysis revealed that genes downregulated in DKO cells were significantly enriched for biological processes reflecting the epithelial-like characteristics of pluripotent cells and featured key regulators such as *NODAL* and *LEFTY* (Fig. 3E). Conversely, genes

upregulated in DKO cells were associated with neural differentiation pathways, including *MAP2* and *WLS* (Fig. 3F).

Collectively, these results indicate that UTX and UTY do not function independently in human ES cells, but instead act redundantly to sustain the expression of pluripotency-associated genes and to prevent premature activation of differentiation programs.

UTX and UTY Regulate the Binding Abilities of OCT4 and SOX2 at Enhancers

The co-occupancy of UTX and UTY at active enhancers prompted us to examine whether their presence influences the binding of OCT4 and SOX2, two core transcription factors essential for maintaining pluripotency. We observed a significant enrichment of OCT4 and SOX2 at regions co-bound by UTX and UTY compared to those occupied by either factor alone (Fig. 4A). When comparing OCT4 binding in wild-type and DKO cells, we observed reduced binding at UTX/UTY co-bound enhancers (<20 kb from TSS) (Fig. 4B). This reduction was more pronounced at enhancers linked to genes downregulated in DKO cells (Fig. 4C,D). A similar decrease was observed for SOX2 binding (Fig. 4E–G), especially at key pluripotency genes such as *LEFTY* and *NODAL* (Fig. 4H,I). Additionally, genes downregulated in DKO cells showed significantly reduced RNA polymerase II loading at their promoters (Supplemental Fig. S4). These results suggest that UTX and UTY together stabilize OCT4 and SOX2 binding and promote promoter activity of target genes.

Depletion of UTX and UTY Results in the Relocation of OCT4 and SOX2

Given that deletion of UTX and UTY reduces OCT4 and SOX2 binding at downregulated genes, we expected the resulting transcriptional changes to resemble those caused by OCT4 depletion. However, comparison of RNA-seq data from DKO cells and OCT4 siRNA-treated cells (Akiyama et al. 2018) revealed minimal overlap in differentially expressed genes (Fig. 5A), suggesting that UTX/UTY loss does not simply reduce OCT4 levels. Indeed, OCT4 expression remained unchanged in UTX/UTY-depleted cells (Fig. 5B).

We therefore investigated whether UTX/UTY loss alters OCT4 genomic binding. Analysis of OCT4 ChIP-seq data using a MA-plot tool (Shao et al. 2012) revealed that although the total number of OCT4 peaks remained largely unchanged, both peak intensities and their genomic locations were dynamically altered in DKO cells (Fig. 5C). Peaks with >2-fold change were

categorized as “lost” or “gained" peaks. OCT4 was redistributed to regions normally unbound in wild-type ES cells—including gene loci such as *TLE4* and *GREB1L*, which are upregulated in DKO cells (Fig. 5C,D). Although some redistribution occurred in single KO cells, it was much more pronounced in DKO cells. A similar pattern was observed for SOX2 (Supplemental Fig. S5). These results indicate that UTX and UTY contribute to the maintenance of proper transcription factor localization across the genome.

To investigate how these altered binding dynamics relate to transcriptional changes, we compared the locations of lost and gained OCT4 peaks with nearby (<20 kb) gene expression changes. Lost OCT4 peaks were frequently located near genes downregulated in DKO cells (Fig. 5E), while gained peaks were associated with upregulated genes (Fig. 5F). These results suggest that UTX and UTY depletion leads to a redistribution of OCT4 binding that directly influences the expression of its target genes.

UTX and UTY Regulate the Localization of Chromatin Remodeling Factors

To explore the mechanisms underlying OCT4 and SOX2 relocation, we examined the distribution of chromatin remodeling factors—MLL4 (a core component of the COMPASS complex), BRG1 (SWI/SNF complex), and CHD7 (an ATP-dependent chromatin remodeler)—in DKO cells. These factors were significantly decreased at sites where OCT4 binding was lost (Fig. 6A,C) and increased at sites where OCT4 binding was gained (Fig. 6B,D). These results suggest that UTX and UTY are important for maintaining the proper localization of chromatin regulatory factors at enhancers.

Consistent with these findings, ATAC-seq and H3K27ac ChIP-seq analyses revealed parallel changes in chromatin accessibility and active chromatin marks (Fig. 6E,F), indicating that alterations in chromatin state likely drive transcription factor redistribution. Importantly, H3K27me3 levels remained unchanged (Supplemental Fig. S6), confirming that UTX and UTY function independently of their histone H3K27 demethylase activity.

The aberrant OCT4 binding observed in UTX- and UTY-deficient cells is likely influenced by the intrinsic properties of the affected genomic regions. Motif analysis of these aberrant OCT4-binding sites revealed enrichment of ZIC1/2 and POU5F1 (OCT4)/SOX2 motifs (Fig. 6G), suggesting these regions are inherently more accessible to transcription factors. This

accessibility may be further increased by chromatin opening caused by UTX and UTY loss, thereby facilitating OCT4 binding.

Together, depletion of UTX and UTY leads to a detrimental loss of enhancer activity and promotes the formation of aberrant active enhancers by impairing the recruitment of chromatin remodeling factors.

UTX and UTY Are Required for Maintenance of Human Pluripotency

To understand how transcriptional dysregulation resulting from the deletion of UTX and UTY affects pluripotency, we performed the teratoma formation assays by injecting UTX-KO, UTY-KO and DKO cells into the subcutaneous tissue of immunodeficient mice (Fig. 7A). Eight weeks after injection, we analyzed the morphology, tissue organization, and gene expression profiles of the resulting tissues. While single KO cells developed teratomas, DKO cells failed to develop recognizable teratomas and only formed small, pale cell masses (Fig. 7B). These results suggest that UTX and UTY are important for maintaining human pluripotency in vivo. Notably, teratomas derived from UTX-KO and UTY-KO cells tended to be smaller than those from WT cells, with the size reduction more pronounced in UTX-KO teratomas, suggesting that differences in demethylase activity between UTX and UTY may begin to exert an influence during teratoma formation.

Histological analysis of the tissue sections revealed that single KO cells generated diverse tissues, including intestinal epithelium, muscle, and neural tubes, whereas DKO cells predominantly differentiated into stromal-like cells (Fig. 7C,D). Further analysis of gene expression related to the three germ layers showed that many genes failed to be upregulated in DKO cells, indicating a marked loss of pluripotency (Fig. 7E). These results suggest that enhancer regulation by UTX and UTY is essential for maintaining pluripotency and supporting human development (Fig. 7F).

Discussion

In this study, we identified the genome-wide binding sites and downstream targets of both UTY and UTX, uncovering their redundant roles in transcriptional regulation in human ES cells. Both proteins regulate the recruitment of chromatin remodeling complexes to enhancers, thereby facilitating proper transcription factor occupancy and maintaining the pluripotent state.

UTY, originally identified as a male-specific antigen (Greenfield et al. 1996), has long lacked a clearly defined function. By contrast, UTX is a well-characterized histone demethylase known to play essential roles in transcriptional activation. This functional distinction is reflected in their disease associations: UTX mutations are linked to disorders such as Kabuki syndrome (Lederer et al. 2012; Banka et al. 2015; Paderova et al. 2016) and acute lymphoblastic leukemia (Mar et al. 2012; Ntziachristos et al. 2014; Van der Meulen et al. 2015; Benyoucef et al. 2016), whereas comparable links for UTY are lacking. Despite these differences, our results show that UTX and UTY perform overlapping roles in chromatin regulation in ES cells, indicating that demethylase activity is not necessary to maintain pluripotency.

Our findings show that UTX and UTY serve as linchpins in stabilizing the binding of transcription factors and chromatin remodeling factors. In the absence of both UTX and UTY, these factors become mislocalized, resulting in impaired enhancer activation and disruption of the gene regulatory network. Crucially, these functions are not mediated by their catalytic demethylase activity. Rather, UTX and UTY involve modulation of chromatin accessibility and histone acetylation. This non-enzymatic function likely depends on domains outside the JmjC domain. In UTX, the TPR domain mediates interaction with the MLL complex promoting transcriptional activation (Kato et al. 2020; Rickels et al. 2020), and a corresponding domain in UTY may support similar functions. Additionally, intrinsically disordered regions (IDRs) in UTX contribute to the recruitment of chromatin remodeling factors via liquid–liquid phase separation (Shi et al. 2021). While UTX-IDR drives a more fluid, liquid-like phase, UTY-IDR tends toward a more solid-like behavior. The relatively low expression of UTY in ES cells may serve to prevent this solid-like behavior from interfering with the dynamic chromatin landscape required for maintaining pluripotency. Thus, UTY compensates for its distinct biophysical properties through reduced expression, thereby achieving a functional outcome comparable to UTX. We cannot exclude the possibility that low UTY expression results in sex-based differences in total UTX/UTY dosage, potentially contributing to functional differences between males and females. Indeed, UTX in male ES cells has been linked to the regulation of female-biased gene expression (Ma et al. 2022).

UTX and UTY bind broadly to enhancer regions across the genome; however, only a subset of nearby genes exhibit transcriptional changes upon their loss. Notably, genes such as NODAL

and LEFTY1/2, which are rapidly repressed during early differentiation (Besser 2004), are among those affected, suggesting that UTX and UTY help maintain transcriptional flexibility at select loci. In contrast, many other target genes remain transcriptionally unchanged, with their chromatin structure appearing stable even in the absence of UTX or UTY. This indicates that transcriptional regulation by UTX and UTY is more nuanced than enhancer occupancy alone. Similarly, general coactivators such as p300, BRD4, and the Mediator complex also exhibit widespread binding yet exert locus-specific effects on transcription (Neumayr et al. 2022). These observations suggest that the presence of regulatory complexes at enhancers is not sufficient for gene activation; rather, transcriptional output depends on a permissive chromatin landscape and appropriate molecular partners. This context dependency likely explains why only a subset of UTX/UTY-bound genes show transcriptional responses upon their loss.

Our study also raises important questions about the timing and requirements of UTX and UTY's catalytic versus non-catalytic functions. In the early stages of development, transcriptional control may rely more on non-enzymatic mechanisms, while enzymatic activity may become essential later for establishing complex transcriptional programs through epigenetic modifications. Thus, functional differences between UTX and UTY may become more pronounced at later stages (Supplemental Fig. S7). Previous studies have shown UTX's demethylase roles in cardiac development (Lee et al. 2012) and in the differentiation of skeletal muscle satellite cells (Seenundun et al. 2010) —functions that UTY cannot substitute for. In contrast, UTX functions in a non-catalytic manner during early developmental stages, such as mesodermal differentiation (Wang et al. 2012) and neural progenitor development (Shan et al. 2020), where UTY may compensate. Indeed, our results show that UTX and UTY relocate to the same enhancer regions during early differentiation of ES cells. This suggests that UTY may function in parallel with UTX during the early stages of differentiation. However, as development advances and cellular diversity increases, UTX and UTY may adopt more distinct and cell type–specific roles. It also remains possible that UTY exerts context-dependent enzymatic functions in certain cell types. Clarifying when and how these proteins function—independently or cooperatively—will be key to understanding their roles in regulating gene expression during tissue-specific differentiation.

Recent evidence shows that concurrent loss of UTX and UTY occurs in multiple human cancer

types (Gozdecka et al. 2018). This study demonstrates that both proteins modulate enhancer function independently of their enzymatic activity, consistent with our findings in human ES cells. Notably, their combined activity suppresses acute myeloid leukemia, suggesting that UTX and UTY regulate transcriptional programs critical for maintaining ES cell identity and preventing tumorigenesis. Shared mechanisms—such as transcriptional plasticity, chromatin accessibility, and enhancer regulation—imply that UTX and UTY operate through a common regulatory framework in both development and cancer progression.

On the other hand, UTY also exhibits unique regulatory roles in certain tissues, indicating the male-specific regulation. UTY participates in prostate development via chromatin remodeling (Dutta et al. 2016), as well as in regulating gene expression in macrophages and epigenetic changes linked to heart failure progression (Horitani et al. 2024). Notably, forced expression of UTY can masculinize gene expression profiles in the placenta and hypothalamus (Rock et al. 2023). Moreover, UTY influences male-specific DNA methylation in valvular interstitial cells (Gorashi et al. 2025), and promotes spermatogonial proliferation to support meiotic sex chromosome pairing (Subrini et al. 2025). Differences in UTX and UTY expression in brain tissue may underlie sex-biased patterns of gene expression (Xu et al. 2008). Thus, the relative importance of the overlapping and distinct functions of UTX and UTY appears to vary depending on the cell type and developmental context. Such functional versatility may underlie the evolutionary pressure to retain UTY on the Y chromosome.

In summary, our findings demonstrate that UTX and UTY safeguard transcription factor localization, a process essential for maintaining pluripotency. Contrary to the notion that UTY has limited function, our results underscore its broader cooperative role with UTX and highlight the significance of Y-linked genes in regulating transcriptional programs in early development.

Materials and Methods

Human ES cell culture and differentiation

The SEES3 hESC line was obtained from the Center for Regenerative Medicine, National Research Institute for Child Health and Development (Japan). Cells were cultured feeder-free in StemFit AK02N medium (Takara) on dishes coated with 0.5 μg/cm² Laminin-511 E8 fragment (iMatrix-511; Takara) at 37 °C in a humidified 5% CO_2 atmosphere. For passaging, cells were dissociated using 50% TrypLE Express (Gibco) with 25 mM EDTA in PBS and

passaged every 4–5 days before reaching 80% confluency; 10 μM Y-27632 (Wako) was added during passaging to promote survival. For endoderm differentiation, dissociated cells were seeded in StemFit medium with Y-27632, then switched the next day to STEMdiff Trilineage Endoderm Medium (Veritas) with daily medium changes for three days. All hESC experiments were approved by the Ethics Committee of Keio University and the Ministry of Education, Culture, Sports, Science and Technology of Japan (October 2012), and by the Ethics Committee of Shiga University of Medical Science for experiments at Yokohama City University (July 2022).

3×Flag-HA knock-in at UTX and UTY loci

Human ES cell lines harboring a C-terminal 3×Flag-HA tag at the endogenous UTX or UTY locus were generated using CRISPR-Cas9 genome editing. For UTX, the donor plasmid included 5′ and 3′ homology arms of 952 bp and 825 bp, respectively, flanking the stop codon. For UTY, the 5′ and 3′ homology arms were 1016 bp and 816 bp, respectively. In both cases, a 3×Flag-HA tag followed by a polyadenylation signal was inserted in-frame at the C-terminus within the 3′ UTR, along with a PGK promoter-driven neomycin resistance cassette containing its own polyA signal. The CRISPR-Cas9 was delivered using the pX330-U6-Chimeric_BB-CBh-hSpCas9 plasmid (Addgene #42230, a gift from Feng Zhang)(Cong et al. 2013), which expresses both Cas9 and sgRNA. ES cells were co-transfected with the Cas9-sgRNA and donor plasmids using GeneJuice Transfection Reagent (Merck), following the manufacturer's instructions. For UTX, the sgRNA target sequence was 5′-AGTACTCTCTCCCGTCCAGT-3′. For UTY, two sgRNAs were used: sgRNA#1, 5′-GGCCATGATGATTACATTTG-3′; and sgRNA#2, 5′-TATTTAATGGCAGTTACGTC-3′. Following selection with 150 μg/ml G418, resistant colonies were isolated and screened by genomic PCR using primers flanking the insertion site. Correct knock-in was confirmed by anti-Flag immunoprecipitation followed by western blotting with anti-UTX or anti-UTY antibodies.

UTX and UTY knockout cell lines

UTX-KO, UTY-KO, and DKO lines were generated using the CRISPR-Cas9. For each gene, two sgRNAs targeting regions downstream of the ATG start codon were designed and cloned into the pX330 plasmid. For UTX, the sgRNA target sequences were 5′-GCCGCTGCCGCCGCCGCTTT-3′and 5′-GCCGCCGTCACTCGCCCGGT-3′. For UTY, the sgRNA sequences were 5′-ACTACCGCCGCTGTTGCCTT-3′and 5′-

CAGACTCCTCTTCACTCTCG-3′. ES cells were co-transfected with the pX330 plasmids and a CAG promoter-driven EGFP-IRES-Puromycin plasmid using GeneJuice. Two days post-transfection, cells were selected with 0.5 μg/ml puromycin and screened for mutations. Genomic DNA was extracted, and the targeted loci were amplified and analyzed by Sanger sequencing to identify insertions or deletions. Clones harboring frameshift mutations resulting in premature stop codons were selected. Two independent clones were established for each genotype. Loss of UTX and UTY protein expression was confirmed by western blotting using anti-UTX and anti-UTY antibodies.

Dual crosslink ChIP

Cells were cross-linked with 2 mM DSG in PBS/1 mM $MgCl_2$ for 40 min at room temperature followed by 1% formaldehyde in PBS for 15 min at room temperature. The reaction was stopped by 125 mM glycine. The cells were washed with PBS and stored at –80°C prior to use. The cells were lysed in Lysis buffer (10 mM Tris-HCl, pH8.0, 1 mM EDTA, 0.5 mM EGTA, 100 mM NaCl, 0.1% Na-Deoxycholate, 0.5% N-lauroyl sarcosine) containing proteinase inhibitor cocktail (Roche). Sonication was conducted with the Handy sonicator UR-21P (Tomy) to generate DNA fragments of approximately 150-450 bp. The sonicated lysates from approximately 2 x 10^6 cells were diluted in ChIP dilution buffer (10 mM HEPES, pH 7.4, 50 mM NaCl, 1% IGEPAL-CA-630, 10% glycerol) containing proteinase inhibitor cocktail and incubated overnight at 4°C with 50 μl of protein G magnetic beads (Invitrogen) that were preincubated with ~2 μg of antibodies. The precipitants were washed once with high salt wash buffer (20 mM Tris-HCl, pH8.0, 400 mM NaCl, 2 mM EDTA, 0.1% SDS, 0.2% Triton-X), three times with LiCl wash buffer (10 mM Tris-HCl, pH 8.0, 1 mM EDTA, 250 mM LiCl, 1% NP40, 1% Na-deoxycholate) and once with 10 mM Tris-HCl, pH 8.0, 5 mM EDTA, 10 mM NaCl. Bound chromatin was eluted in elution buffer (90 mM $NaHCO_3$, 1% SDS), and crosslinks were reversed by adding a 1:5 dilution of decross-linking buffer (2 M NaCl, 0.1 M EDTA, 0.4 M Tris-HCl, pH 6.8) and incubating at 65°C for 3 h. Samples were treated with RNase A at 37°C for 30 minutes and proteinase K at 55°C for 1 h. DNA was purified using phenol-chloroform-isoamyl alcohol extraction followed by ethanol precipitation.

ChIP-seq library preparation and sequencing

ChIP DNA libraries were prepared using the NEBNext ChIP-Seq Library Prep Kit for Illumina (NEB) according to the manufacturer's instructions. Sequencing was performed on an Illumina

HiSeq 2500 platform (50 bp, single-end).

Processing and analysis of ChIP-seq data

Raw sequencing reads were quality-controlled and trimmed using Fastp to remove adapter sequences and low-quality bases. The resulting reads were aligned to the human reference genome (GRCh38) using Bowtie2 with default parameters. Aligned reads were processed using SAMtools to generate BAM and index files. Peak calling was performed with MACS2 in narrowPeak mode using a q-value cutoff of < 0.05. For each condition, peaks identified from three independent biological replicates were merged, retaining only those located on autosomes (chromosomes 1–22) and sex chromosomes (X and Y). Peaks detected uniquely in only one replicate with abnormally high signal were excluded. BAM files from the three replicates were merged for downstream analysis. Differential peak analysis was conducted using MAnorm with default parameters. To compare peak locations between conditions, genomic distances were computed using bedtools closest. For visualization, bamCoverage was used to generate BigWig files with counts per million normalization. These tracks were visualized using the Integrative Genomics Viewer. Signal differences between conditions were assessed using bigwigCompare. Heatmaps and aggregation plots were created using deepTools computeMatrix, followed by visualization with plotHeatmap and plotProfile. De novo and known motif enrichment analyses were performed using HOMER with a 200 bp window size and the -mask option to exclude repetitive sequences. Genomic annotations of peaks relative to TSS and gene bodies were obtained using HOMER annotatePeaks.pl. Gene set enrichment analysis (GSEA) was conducted to assess the association between OCT4 binding and gene expression changes.

RNA-seq library preparation and sequencing

RNA-seq libraries were prepared from 500 ng of total RNA per sample using the NEBNext Poly(A) mRNA Magnetic Isolation Module, followed by the NEBNext Ultra II Directional RNA Library Prep Kit for Illumina (NEB), according to the manufacturer's protocols. Sequencing was performed on an Illumina HiSeq 2500 platform using single-end 50 bp reads.

Processing and analysis of RNA-seq data

Sequence reads were aligned to the human genome (GRCh38) using STAR. TPM and FPKM values were estimated using RSEM. Gene-level expression was also quantified using featureCounts based on the annotation file Homo_sapiens.GRCh38.105.gtf. For differential

expression analysis, raw counts obtained by featureCounts were analyzed using the TCC-GUI pipeline in R. Two independent biological replicates were used for comparisons. Normalization was performed using the TMM method, and differentially expressed genes were identified using edgeR. Genes with a $\log_2$ fold change > 1 and a p-value < 0.05 were considered significantly differentially expressed.

ATAC-seq

ATAC-seq was performed using the Omni-ATAC protocol (Corces et al. 2017) with minor modifications. Briefly, 1×10^5 viable cells were resuspended in 50 µl of cold ATAC Resuspension Buffer (RSB)(10 mM Tris-HCl (pH 7.4), 10 mM NaCl, and 3 mM $MgCl_2$) containing 0.1% NP-40, 0.1% Tween-20, and 0.01% digitonin. After incubation on ice for 3 min, cells were washed with 1 ml of cold RSB containing 0.1% Tween-20, and nuclei were pelleted at 500 × g for 10 min at 4°C. The nuclear pellet was resuspended in 50 µl of transposition mix (25 µl of 2× TD buffer (20 mM Tris-HCl, pH 7.6; 10 mM $MgCl_2$; 20% dimethylformamide), 2.5 µl of Tn5 transposase, 16.9 µl of PBS, 0.5 µl of 10% Tween-20, 0.1 µl of digitonin, and 5 µl of water), and incubated at 37°C for 30 min in a thermomixer at 630 rpm. Transposed DNA was purified with AMPure XP beads (1.8×) and eluted in 20 µl of EB buffer. Libraries were pre-amplified with NEBNext High-Fidelity 2X PCR Master Mix for 5 cycles, and 10% of the reaction was used in a qPCR side reaction to determine the required number of additional cycles. Final amplification was performed with the remaining reaction, and PCR products were purified using a two-step AMPure XP bead cleanup (0.6× followed by 1.3×). Final libraries were eluted in 20 µl of EB buffer and assessed using a Bioanalyzer (Agilent) to confirm fragment size distribution.

Teratoma formation assay

Human ES cells were dissociated into single cells and resuspended in a 1:2 mixture of Matrigel (Corning) and StemFit AK02N medium supplemented with 10 µM Y-27632. A total of 1×10^6 cells in 100 µL of this mixture were subcutaneously injected into the dorsal flank of immunodeficient SCID mice (CLEA Japan). After 8 weeks, the mice were sacrificed, and the injection sites were dissected to assess teratoma formation. The excised tissues were fixed in 4% paraformaldehyde, embedded in paraffin, and sectioned for histological and immunohistochemical analyses. All animal procedures were approved by the Animal Care and Use Committee of Keio University School of Medicine.

Quantification and statistical analysis

Descriptive and comparative statistics were performed as detailed in the figure legends with the number of replicates indicated. Significance is defined as a p-value less than 0.05 indicated with asterisk. Error bar represents the standard deviation of the mean of the replicates. Statistical analyses were implemented with Prism 9 (GraphPad) or Excel (Microsoft) software.

Data availability

All sequencing data have been deposited in the GEO database under series accession number GSE301298.

Oligonucleotides and antibodies

The oligonucleotide primers and antibodies used in this study are listed in Supplemental Table S1.

Competing interest statement

The authors declare no competing interests.

Acknowledgments

We thank the members of our laboratory and the Collaborative Research Resources, Keio University, for technical assistance. We also thank Hitoshi Niwa of Kumamoto university for kindly providing the SOX2 antibody. This work was supported by grants from the Japan Society for the Promotion of Science (JSPS) Grant-in-Aid for Specially Promoted Research (JP19K06492, JP20H05395, JP20H04929, JP22K06090, JP22H04699 to T.A.).

Author contributions

T.A. conceived the project, performed the experiments, and analyzed the data. S.S. and M.Y. performed experiments, and T.N. and M.Y. analyzed the NGS data. K.I. contributed to the generation of knock-in cells. H.T. contributed to the data analysis. T.A. and M.S.H.K. supervised the project and interpreted the results. T.A. wrote the manuscript with feedback from co-authors.

References

Agger K, Cloos PA, Christensen J, Pasini D, Rose S, Rappsilber J, Issaeva I, Canaani E, Salcini AE, Helin K. 2007. UTX and JMJD3 are histone H3K27 demethylases involved in HOX gene regulation and development. *Nature* **449**: 731-734.

Akiyama T, Sato S, Chikazawa-Nohtomi N, Soma A, Kimura H, Wakabayashi S, Ko SBH, Ko MSH. 2018. Efficient differentiation of human pluripotent stem cells into skeletal muscle cells by combining RNA-based MYOD1-expression and POU5F1-silencing. *Sci Rep* **8**: 1189.

Akiyama T, Wakabayashi S, Soma A, Sato S, Nakatake Y, Oda M, Murakami M, Sakota M, Chikazawa-Nohtomi N, Ko SB et al. 2016. Transient ectopic expression of the histone demethylase JMJD3 accelerates the differentiation of human pluripotent stem cells. *Development* **143**: 3674-3685.

Banka S, Lederer D, Benoit V, Jenkins E, Howard E, Bunstone S, Kerr B, McKee S, Lloyd IC, Shears D et al. 2015. Novel KDM6A (UTX) mutations and a clinical and molecular review of the X-linked Kabuki syndrome (KS2). *Clin Genet* **87**: 252-258.

Bellott DW, Hughes JF, Skaletsky H, Brown LG, Pyntikova T, Cho TJ, Koutseva N, Zaghlul S, Graves T, Rock S et al. 2014. Mammalian Y chromosomes retain widely expressed dosage-sensitive regulators. *Nature* **508**: 494-499.

Bellott DW, Skaletsky H, Pyntikova T, Mardis ER, Graves T, Kremitzki C, Brown LG, Rozen S, Warren WC, Wilson RK et al. 2010. Convergent evolution of chicken Z and human X chromosomes by expansion and gene acquisition. *Nature* **466**: 612-616.

Benyoucef A, Palii CG, Wang C, Porter CJ, Chu A, Dai F, Tremblay V, Rakopoulos P, Singh K, Huang S et al. 2016. UTX inhibition as selective epigenetic therapy against TAL1-driven T-cell acute lymphoblastic leukemia. *Genes Dev* **30**: 508-521.

Besser D. 2004. Expression of nodal, lefty-a, and lefty-B in undifferentiated human embryonic stem cells requires activation of Smad2/3. *J Biol Chem* **279**: 45076-45084.

Burgold T, Spreafico F, De Santa F, Totaro MG, Prosperini E, Natoli G, Testa G. 2008. The histone H3 lysine 27-specific demethylase Jmjd3 is required for neural commitment. *PLoS One* **3**: e3034.

Cong L, Ran FA, Cox D, Lin S, Barretto R, Habib N, Hsu PD, Wu X, Jiang W, Marraffini LA et al. 2013. Multiplex genome engineering using CRISPR/Cas systems. *Science* **339**: 819-823.

Corces MR, Trevino AE, Hamilton EG, Greenside PG, Sinnott-Armstrong NA, Vesuna S, Satpathy AT, Rubin AJ, Montine KS, Wu B et al. 2017. An improved ATAC-seq protocol reduces background and enables interrogation of frozen tissues. *Nat Methods* **14**: 959-962.

Dutta A, Le Magnen C, Mitrofanova A, Ouyang X, Califano A, Abate-Shen C. 2016. Identification of

an NKX3.1-G9a-UTY transcriptional regulatory network that controls prostate differentiation. *Science* **352**: 1576-1580.

Gazova I, Lengeling A, Summers KM. 2019. Lysine demethylases KDM6A and UTY: The X and Y of histone demethylation. *Mol Genet Metab* **127**: 31-44.

Godfrey AK, Naqvi S, Chmatal L, Chick JM, Mitchell RN, Gygi SP, Skaletsky H, Page DC. 2020. Quantitative analysis of Y-Chromosome gene expression across 36 human tissues. *Genome Res* **30**: 860-873.

Gorashi RM, Baddour T, Chittle SJ, Felix Velez NE, Wenning MA, Anseth KS, Mestroni L, Pena B, Guo P, Aguado BA. 2025. Y chromosome-linked UTY modulates sex differences in valvular fibroblast methylation in response to nanoscale extracellular matrix cues. *Sci Adv* **11**: eads5717.

Gozdecka M, Meduri E, Mazan M, Tzelepis K, Dudek M, Knights AJ, Pardo M, Yu L, Choudhary JS, Metzakopian E et al. 2018. UTX-mediated enhancer and chromatin remodeling suppresses myeloid leukemogenesis through noncatalytic inverse regulation of ETS and GATA programs. *Nat Genet* **50**: 883-894.

Greenfield A, Carrel L, Pennisi D, Philippe C, Quaderi N, Siggers P, Steiner K, Tam PP, Monaco AP, Willard HF et al. 1998. The UTX gene escapes X inactivation in mice and humans. *Hum Mol Genet* **7**: 737-742.

Greenfield A, Scott D, Pennisi D, Ehrmann I, Ellis P, Cooper L, Simpson E, Koopman P. 1996. An H-YDb epitope is encoded by a novel mouse Y chromosome gene. *Nat Genet* **14**: 474-478.

Hong S, Cho YW, Yu LR, Yu H, Veenstra TD, Ge K. 2007. Identification of JmjC domain-containing UTX and JMJD3 as histone H3 lysine 27 demethylases. *Proc Natl Acad Sci U S A* **104**: 18439-18444.

Horitani K, Chavkin NW, Arai Y, Wang Y, Ogawa H, Yura Y, Evans MA, Cochran JD, Thel MC, Polizio AH et al. 2024. Disruption of the Uty epigenetic regulator locus in hematopoietic cells phenocopies the profibrotic attributes of Y chromosome loss in heart failure. *Nat Cardiovasc Res* **3**: 343-355.

Hughes JF, Page DC. 2015. The Biology and Evolution of Mammalian Y Chromosomes. *Annu Rev Genet* **49**: 507-527.

Hughes JF, Skaletsky H, Brown LG, Pyntikova T, Graves T, Fulton RS, Dugan S, Ding Y, Buhay CJ, Kremitzki C et al. 2012. Strict evolutionary conservation followed rapid gene loss on human and rhesus Y chromosomes. *Nature* **483**: 82-86.

Hughes JF, Skaletsky H, Pyntikova T, Minx PJ, Graves T, Rozen S, Wilson RK, Page DC. 2005. Conservation of Y-linked genes during human evolution revealed by comparative sequencing in

chimpanzee. *Nature* **437**: 100-103.

Kartikasari AE, Zhou JX, Kanji MS, Chan DN, Sinha A, Grapin-Botton A, Magnuson MA, Lowry WE, Bhushan A. 2013. The histone demethylase Jmjd3 sequentially associates with the transcription factors Tbx3 and Eomes to drive endoderm differentiation. *EMBO J* **32**: 1393-1408.

Kato H, Asamitsu K, Sun W, Kitajima S, Yoshizawa-Sugata N, Okamoto T, Masai H, Poellinger L. 2020. Cancer-derived UTX TPR mutations G137V and D336G impair interaction with MLL3/4 complexes and affect UTX subcellular localization. *Oncogene* **39**: 3322-3335.

Klose RJ, Kallin EM, Zhang Y. 2006. JmjC-domain-containing proteins and histone demethylation. *Nat Rev Genet* **7**: 715-727.

Lahn BT, Page DC. 1999. Four evolutionary strata on the human X chromosome. *Science* **286**: 964-967.

Lederer D, Grisart B, Digilio MC, Benoit V, Crespin M, Ghariani SC, Maystadt I, Dallapiccola B, Verellen-Dumoulin C. 2012. Deletion of KDM6A, a histone demethylase interacting with MLL2, in three patients with Kabuki syndrome. *Am J Hum Genet* **90**: 119-124.

Lederer D, Shears D, Benoit V, Verellen-Dumoulin C, Maystadt I. 2014. A three generation X-linked family with Kabuki syndrome phenotype and a frameshift mutation in KDM6A. *Am J Med Genet A* **164A**: 1289-1292.

Lee S, Lee JW, Lee SK. 2012. UTX, a histone H3-lysine 27 demethylase, acts as a critical switch to activate the cardiac developmental program. *Dev Cell* **22**: 25-37.

Lei X, Jiao J. 2018. UTX Affects Neural Stem Cell Proliferation and Differentiation through PTEN Signaling. *Stem Cell Reports* **10**: 1193-1207.

Ma W, Fang H, Pease N, Filippova GN, Disteche CM, Berletch JB. 2022. Sex-biased and parental allele-specific gene regulation by KDM6A. *Biol Sex Differ* **13**: 40.

Mansour AA, Gafni O, Weinberger L, Zviran A, Ayyash M, Rais Y, Krupalnik V, Zerbib M, Amann-Zalcenstein D, Maza I et al. 2012. The H3K27 demethylase Utx regulates somatic and germ cell epigenetic reprogramming. *Nature* **488**: 409-413.

Mar BG, Bullinger L, Basu E, Schlis K, Silverman LB, Dohner K, Armstrong SA. 2012. Sequencing histone-modifying enzymes identifies UTX mutations in acute lymphoblastic leukemia. *Leukemia* **26**: 1881-1883.

Mueller JL, Skaletsky H, Brown LG, Zaghlul S, Rock S, Graves T, Auger K, Warren WC, Wilson RK, Page DC. 2013. Independent specialization of the human and mouse X chromosomes for the male germ line. *Nat Genet* **45**: 1083-1087.

Nakatake Y, Ko SBH, Sharov AA, Wakabayashi S, Murakami M, Sakota M, Chikazawa N, Ookura C,

Sato S, Ito N et al. 2020. Generation and Profiling of 2,135 Human ESC Lines for the Systematic Analyses of Cell States Perturbed by Inducing Single Transcription Factors. *Cell Rep* **31**: 107655.

Neumayr C, Haberle V, Serebreni L, Karner K, Hendy O, Boija A, Henninger JE, Li CH, Stejskal K, Lin G et al. 2022. Differential cofactor dependencies define distinct types of human enhancers. *Nature* **606**: 406-413.

Ntziachristos P, Tsirigos A, Welstead GG, Trimarchi T, Bakogianni S, Xu L, Loizou E, Holmfeldt L, Strikoudis A, King B et al. 2014. Contrasting roles of histone 3 lysine 27 demethylases in acute lymphoblastic leukaemia. *Nature* **514**: 513-517.

Paderova J, Holubova A, Simandlova M, Puchmajerova A, Vlckova M, Malikova M, Pourova R, Vejvalkova S, Havlovicova M, Senkerikova M et al. 2016. Molecular genetic analysis in 14 Czech Kabuki syndrome patients is confirming the utility of phenotypic scoring. *Clin Genet* **90**: 230-237.

Rickels R, Wang L, Iwanaszko M, Ozark PA, Morgan MA, Piunti A, Khalatyan N, Soliman SHA, Rendleman EJ, Savas JN et al. 2020. A small UTX stabilization domain of Trr is conserved within mammalian MLL3-4/COMPASS and is sufficient to rescue loss of viability in null animals. *Genes Dev* **34**: 1493-1502.

Rock KD, Folts LM, Zierden HC, Marx-Rattner R, Leu NA, Nugent BM, Bale TL. 2023. Developmental transcriptomic patterns can be altered by transgenic overexpression of Uty. *Sci Rep* **13**: 21082.

Seenundun S, Rampalli S, Liu QC, Aziz A, Palii C, Hong S, Blais A, Brand M, Ge K, Dilworth FJ. 2010. UTX mediates demethylation of H3K27me3 at muscle-specific genes during myogenesis. *EMBO J* **29**: 1401-1411.

Shan Y, Zhang Y, Zhao Y, Wang T, Zhang J, Yao J, Ma N, Liang Z, Huang W, Huang K et al. 2020. JMJD3 and UTX determine fidelity and lineage specification of human neural progenitor cells. *Nat Commun* **11**: 382.

Shao Z, Zhang Y, Yuan GC, Orkin SH, Waxman DJ. 2012. MAnorm: a robust model for quantitative comparison of ChIP-Seq data sets. *Genome Biol* **13**: R16.

Shi B, Li W, Song Y, Wang Z, Ju R, Ulman A, Hu J, Palomba F, Zhao Y, Le JP et al. 2021. UTX condensation underlies its tumour-suppressive activity. *Nature* **597**: 726-731.

Shpargel KB, Sengoku T, Yokoyama S, Magnuson T. 2012. UTX and UTY demonstrate histone demethylase-independent function in mouse embryonic development. *PLoS Genet* **8**: e1002964.

Skaletsky H, Kuroda-Kawaguchi T, Minx PJ, Cordum HS, Hillier L, Brown LG, Repping S, Pyntikova T, Ali J, Bieri T et al. 2003. The male-specific region of the human Y chromosome is a mosaic of discrete sequence classes. *Nature* **423**: 825-837.

Subrini J, Varsally W, Balsells IB, Bensberg M, Sioutas G, Ojarikre O, Maciulyte V, Gylemo B, Crawley K, Courtis K et al. 2025. Systematic identification of Y-chromosome gene functions in mouse spermatogenesis. *Science* **387**: 393-400.

Tang QY, Zhang SF, Dai SK, Liu C, Wang YY, Du HZ, Teng ZQ, Liu CM. 2020. UTX Regulates Human Neural Differentiation and Dendritic Morphology by Resolving Bivalent Promoters. *Stem Cell Reports* **15**: 439-453.

Theunissen TW, Friedli M, He Y, Planet E, O'Neil RC, Markoulaki S, Pontis J, Wang H, Iouranova A, Imbeault M et al. 2016. Molecular Criteria for Defining the Naive Human Pluripotent State. *Cell Stem Cell* **19**: 502-515.

Tian B, Yang J, Brasier AR. 2012. Two-step cross-linking for analysis of protein-chromatin interactions. *Methods Mol Biol* **809**: 105-120.

Van der Meulen J, Sanghvi V, Mavrakis K, Durinck K, Fang F, Matthijssens F, Rondou P, Rosen M, Pieters T, Vandenberghe P et al. 2015. The H3K27me3 demethylase UTX is a gender-specific tumor suppressor in T-cell acute lymphoblastic leukemia. *Blood* **125**: 13-21.

Walport LJ, Hopkinson RJ, Vollmar M, Madden SK, Gileadi C, Oppermann U, Schofield CJ, Johansson C. 2014. Human UTY(KDM6C) is a male-specific Nϵ-methyl lysyl demethylase. *J Biol Chem* **289**: 18302-18313.

Wang C, Lee JE, Cho YW, Xiao Y, Jin Q, Liu C, Ge K. 2012. UTX regulates mesoderm differentiation of embryonic stem cells independent of H3K27 demethylase activity. *Proc Natl Acad Sci U S A* **109**: 15324-15329.

Wang SP, Tang Z, Chen CW, Shimada M, Koche RP, Wang LH, Nakadai T, Chramiec A, Krivtsov AV, Armstrong SA et al. 2017. A UTX-MLL4-p300 Transcriptional Regulatory Network Coordinately Shapes Active Enhancer Landscapes for Eliciting Transcription. *Mol Cell* **67**: 308-321 e306.

Wei Y, Wang T, Ma L, Zhang Y, Zhao Y, Lye K, Xiao L, Chen C, Wang Z, Ma Y et al. 2021. Efficient derivation of human trophoblast stem cells from primed pluripotent stem cells. *Sci Adv* **7**.

Welstead GG, Creyghton MP, Bilodeau S, Cheng AW, Markoulaki S, Young RA, Jaenisch R. 2012. X-linked H3K27me3 demethylase Utx is required for embryonic development in a sex-specific manner. *Proc Natl Acad Sci U S A* **109**: 13004-13009.

Xu J, Deng X, Watkins R, Disteche CM. 2008. Sex-specific differences in expression of histone

demethylases Utx and Uty in mouse brain and neurons. *J Neurosci* **28**: 4521-4527.

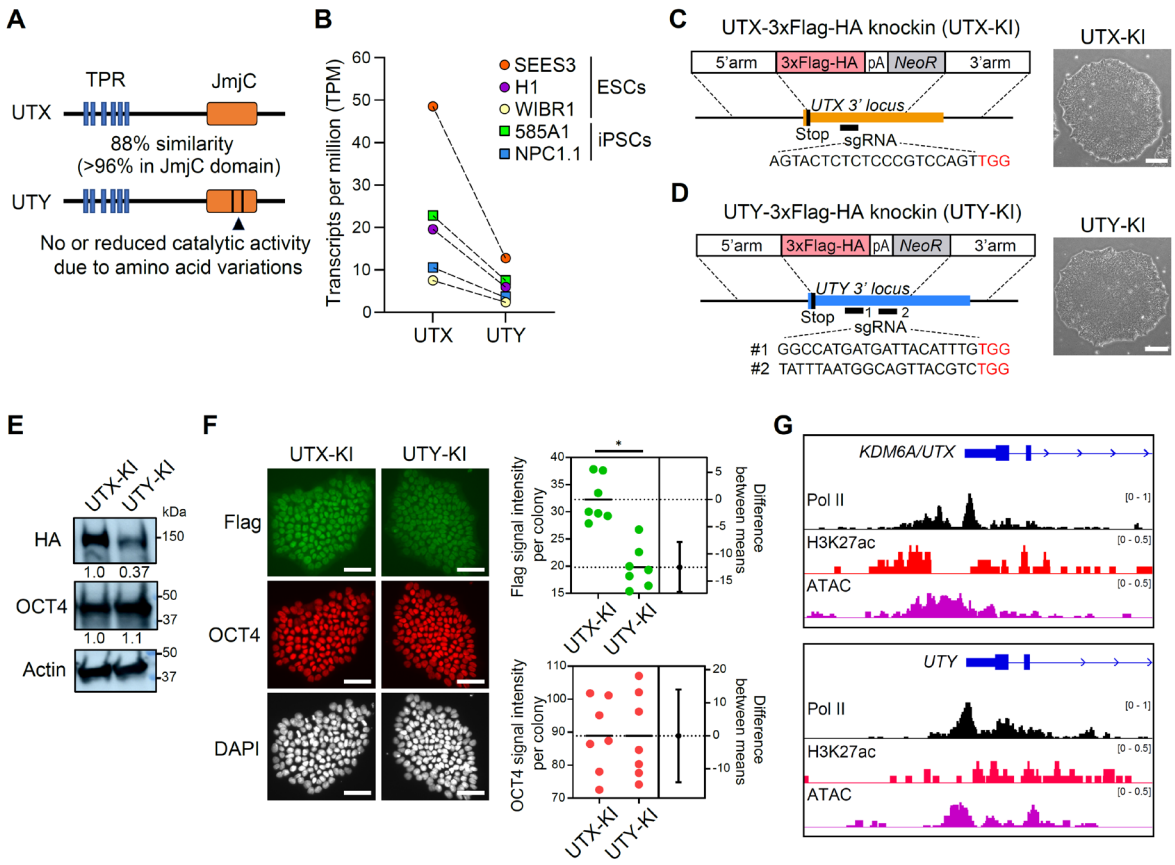

Figure 1. UTY is expressed at lower levels than UTX in human pluripotent stem cells
(A) Domain organization of UTX and UTY. TPR, tetratricopeptide repeat; JmjC, Jumonji C domain. (B) Comparison of RNA expression levels of UTX and UTY in human pluripotent stem cell lines. Transcripts per million (TPM) values are shown for ES cell lines (SEES3, H1, WIBR1) and iPS cell lines (585A1, NPC1.1). (C, D) CRISPR-Cas9 was used to generate UTX-3xFlag-HA and UTY-3xFlag-HA knock-in (UTX-KI and UTY-KI) human ES cells by inserting a 3xFlag-HA tag at the C-terminus of each gene. sgRNA target sequences are shown in black, and PAM sequences are shown in red. (E) Protein expression levels of UTX and UTY were assessed by immunoblotting using an HA antibody. ACTB antibodies were used as loading controls. The values indicate HA and OCT4 signal intensities normalized by ACTB signals. (F) Immunostaining analysis using a Flag antibody in UTX-KI and UTY-KI cells. The signal intensities of ES colonies ($N = 7$) were quantified. *$P < 0.01$ by one-sided Student's t-test. The OCT4 staining intensities were used as a control. Nuclei were counterstained with DAPI. (G) Profiles of Pol II, H3K27ac, and ATAC-seq signals at the promoter regions of the UTX and UTY genes.

Akiyama_Fig.2

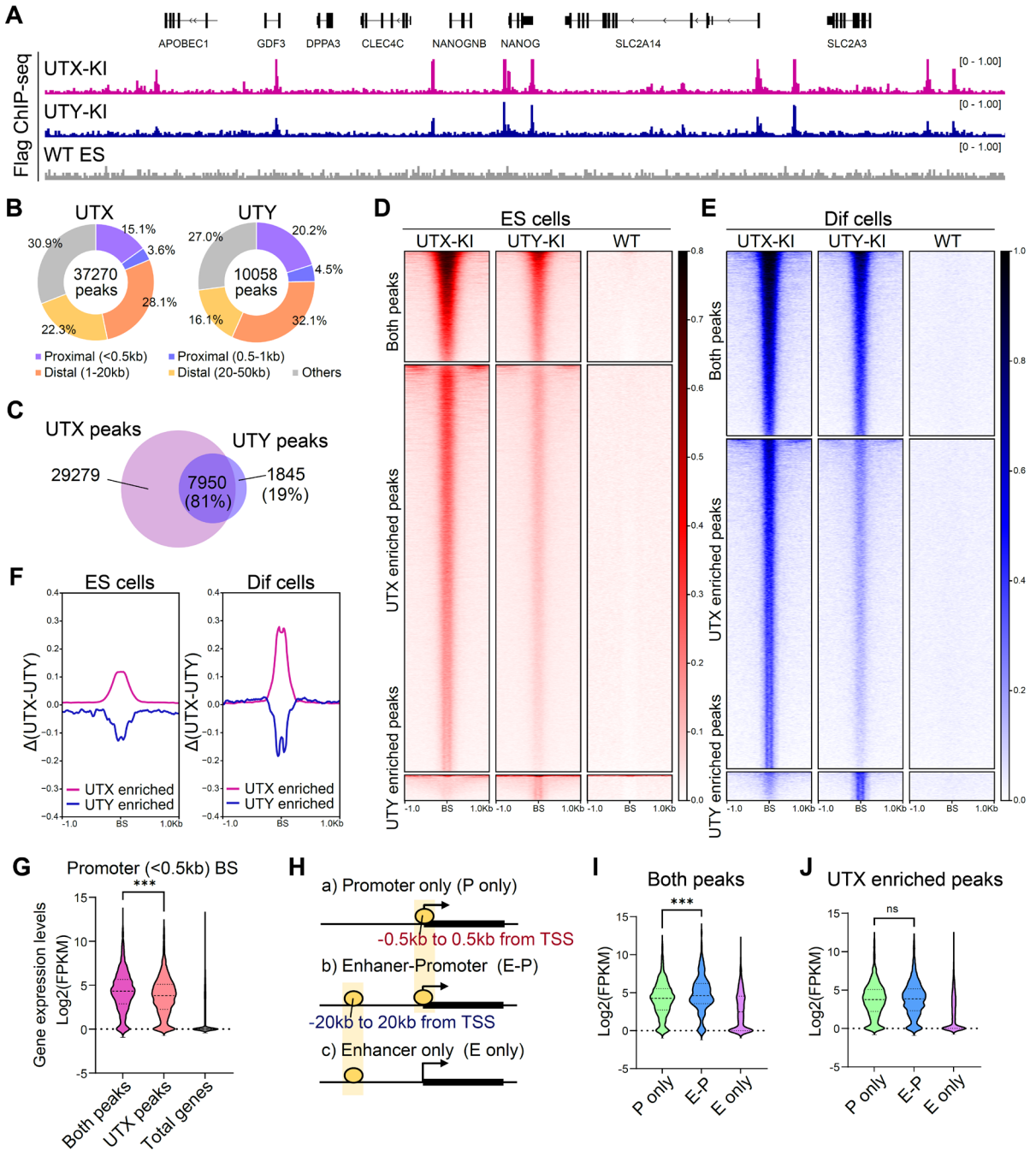

Figure 2. UTY is co-localized with UTX at promoters and enhancers in active genes

(A) ChIP-seq tracks representing UTX and UTY localization patterns in ES cells. ChIP-seq analysis was performed using a Flag antibody in UTX-KI and UTY cells. Wild-type ES cells were used as a negative control. (B) Number of the UTX and UTY ChIP-seq peaks and their distribution relative to the TSS. (C) Overlapping of the UTX and UTY ChIP-seq peaks. (D) Flag ChIP-seq signal intensities of UTX-KI and UTY-KI cells are shown within a 2 kb region centered on the sites of both peaks, UTX-enriched peaks, and UTY-enriched peaks in ES cells. Flag ChIP-seq signal intensities of wild-type ES cells were used as a negative control. (E) ChIP-seq signal intensities of UTX-KI and UTY-KI within a 2 kb region centered on the sites of both peaks, UTX-enriched peaks, and UTY-enriched peaks in differentiated cells. Wild-type ES cells were used as a negative control. (F) Differences of UTX and UTY ChIP-seq signal intensities at UTX-enriched sites and UTY-enriched sites in ES cells and differentiated cells. (G) Gene expression levels of genes with both peaks or UTX-enriched peaks at promoter regions. Total genes are used as a control. $*P < 0.01$ by one-sided Student's t-test. (H) Localization patterns related to gene regulation: a) promoter only, b) enhancer and promoter, c) enhancer only. (I) Gene expression levels of genes with both peaks at the three localization patterns. $*P < 0.01$ by one-sided Student's t-test. (J) Gene expression levels of genes with UTX peaks at the three localization patterns. 'ns' indicates not significant.

Akiyama_Fig.3

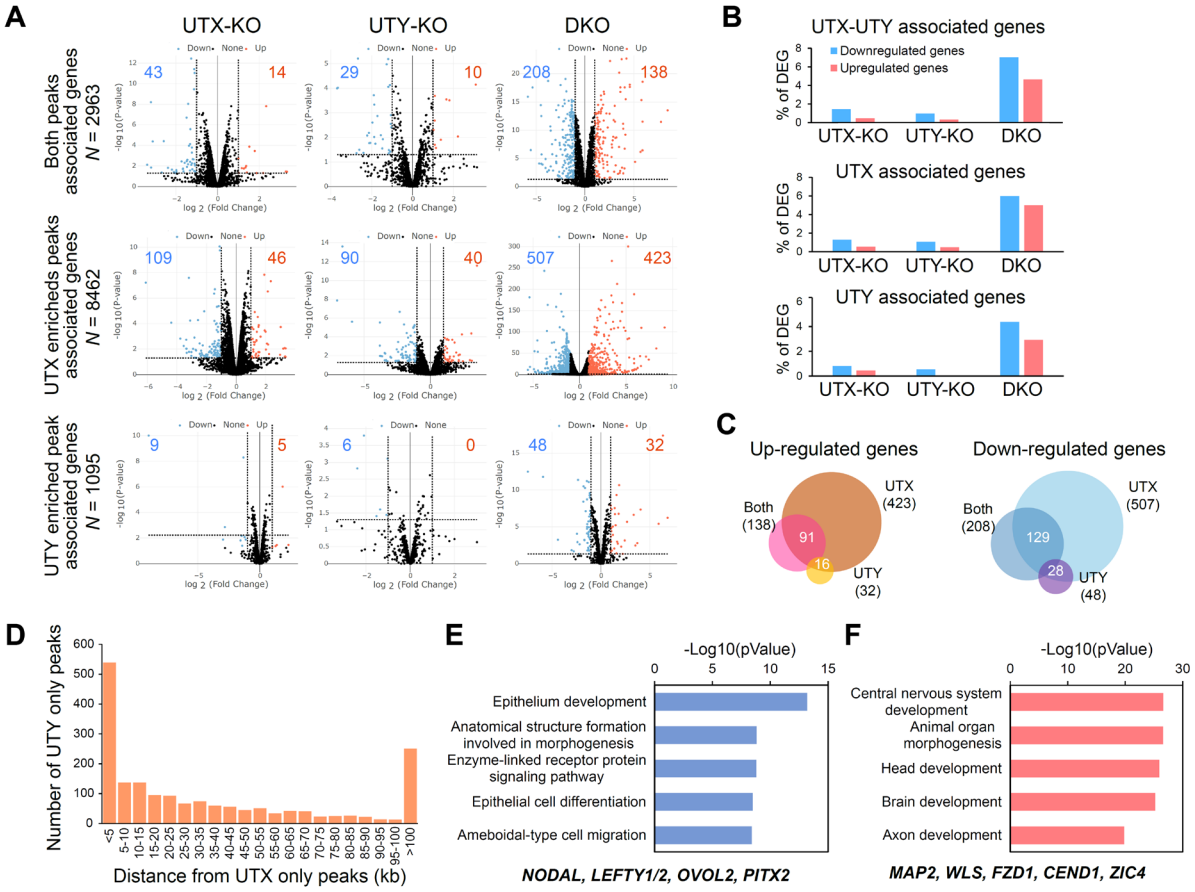

Figure 3. Genes expression changes in UTX-KO, UTY-KO, and DKO cells.

(A) Gene expression changes in UTX-KO, UTY-KO, and DKO cells are shown with volcano plots. Blue plots indicate downregulated genes, and red plots indicate upregulated genes. Th graphs are shown separately for genes associated with both peaks (genes within 20 kb of the peaks), UTX-enriched peaks, and UTY-enriched peaks. (B) The percentage of differentially expressed genes (DEGs) are summarized. (C) Overlapping of DEGs associated with both, UTX-enriched, and UTY-enriched peaks. (D) The relationship between UTX peaks and UTY peaks. A graph showing the number of UTY peaks located at the indicated distances from UTX peaks. (E) Characterization of downregulated genes in DKO cells. Example genes are shown. (F) Characterization of upregulated genes in DKO cells. Example genes are shown.

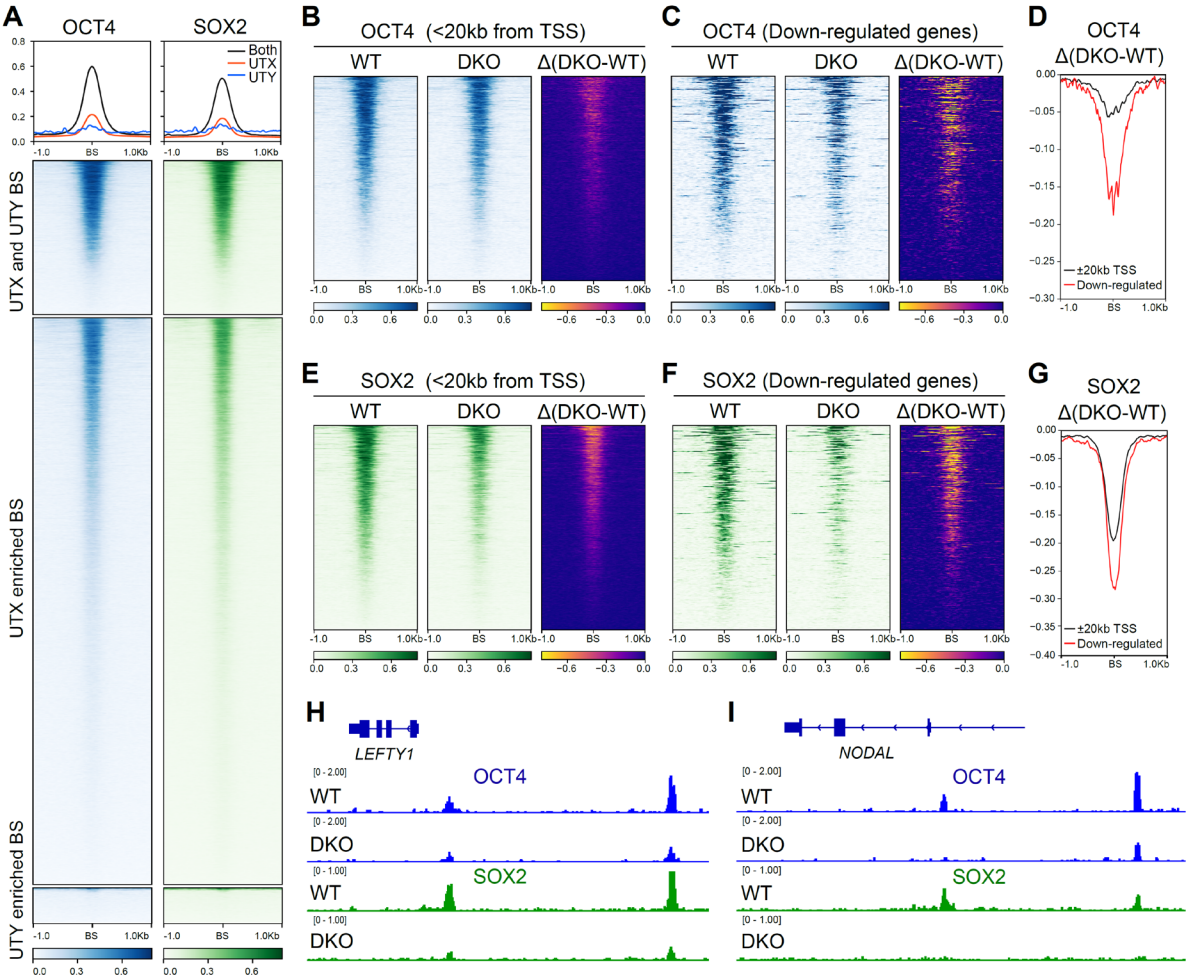

Figure 4. UTX/UTY DKO impairs the binding of OCT4 and SOX2 at active enhancers
(A) ChIP-seq signal intensities of OCT4 and SOX2 centered (±1 kb) on UTX/UTY (both), UTX-enriched, and UTY-enriched binding sites. (B) OCT4 ChIP-seq signals in WT and DKO cells centered on UTX/UTY binding sites located within 20 kb of TSS. Signal differences between WT and DKO also shown. (C) Same as (B), but restricted to binding sites near genes downregulated in DKO cells. (D) Comparison of OCT4Δ(DKO–WT) signals at UTX/UTY binding sites within 20 kb of the TSS of all genes versus downregulated genes. (E) SOX2 ChIP-seq signals in WT and DKO cells centered on UTX/UTY binding sites within 20 kb of TSS, with differences shown. (F) Same as (E), but focused on sites near downregulated genes. (G) Comparison of SOX2Δ(DKO–WT) signals within 20 kb of the TSS of all genes versus downregulated genes. (H, I) Reduced OCT4 and SOX2 binding at the *LEFTY1* and *NODAL* loci in DKO cells.

Akiyama_Fig.5

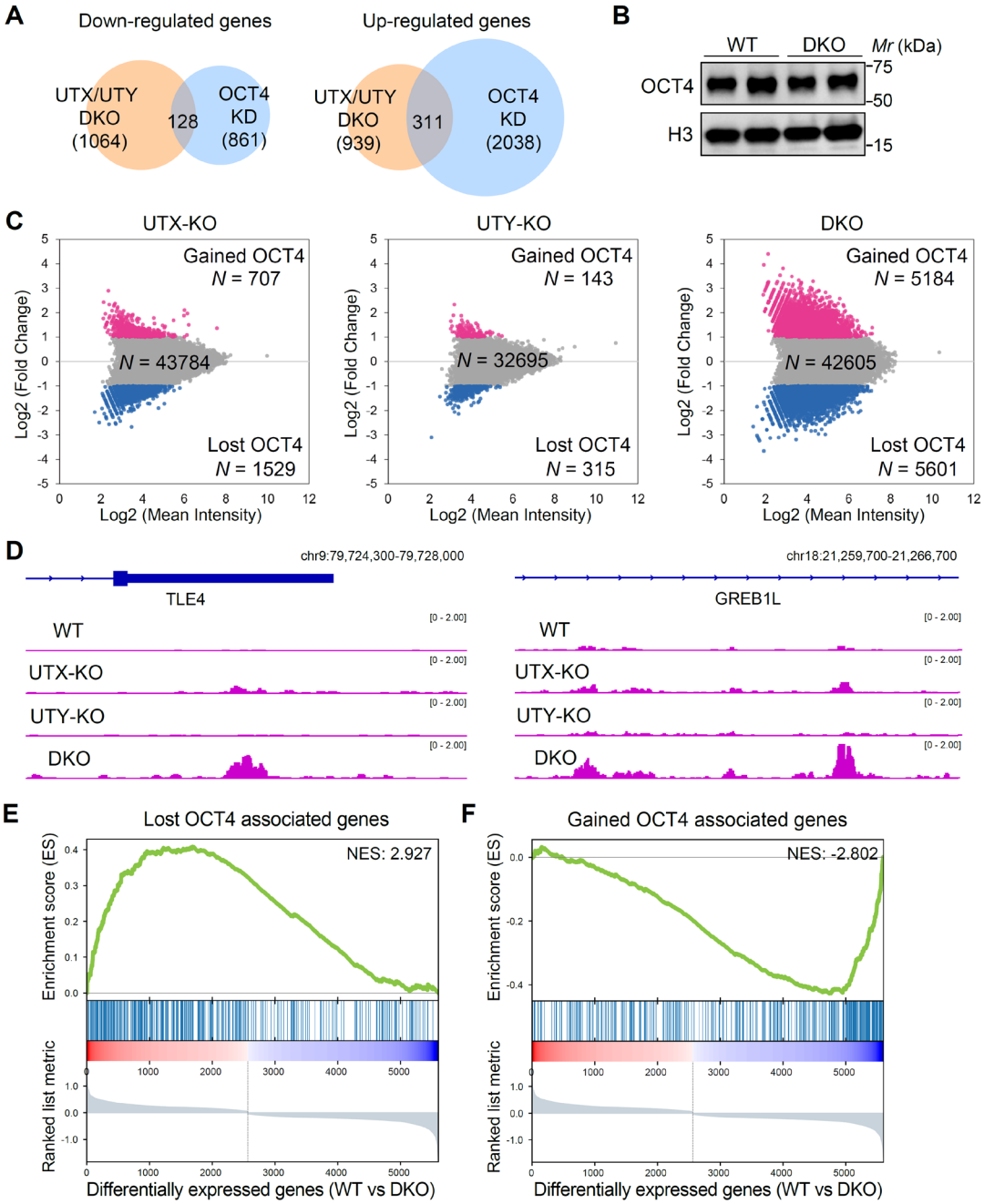

Figure 5. UTX/UTY DKO results in the relocation of OCT4

(A) Comparison of differentially expressed genes between UTX/UTY DKO cells and OCT4 KD (knockdown) cells. (B) Immunoblotting analysis showing that OCT4 levels remain unchanged between WT and DKO cells. Histone H3 is used as a loading control. (C) Differences in OCT4 distribution patterns in UTX-KO, UTY-KO, and DKO cells compared to WT cells. Increased ChIP-seq peaks, indicating gained OCT4 binding, are shown in pink, while decreased ChIP-seq peaks, indicating lost OCT4 binding, are shown in blue. (D) Examples of increased OCT4 peaks in DKO cells. (E,F) The relationship between genes associated with altered OCT4 levels and genes whose expression is changed by DKO. Lost OCT4 site-associated genes are enriched in genes downregulated in DKO cells (E), whereas gained OCT4 site-associated genes are enriched in genes upregulated in DKO cells (F).

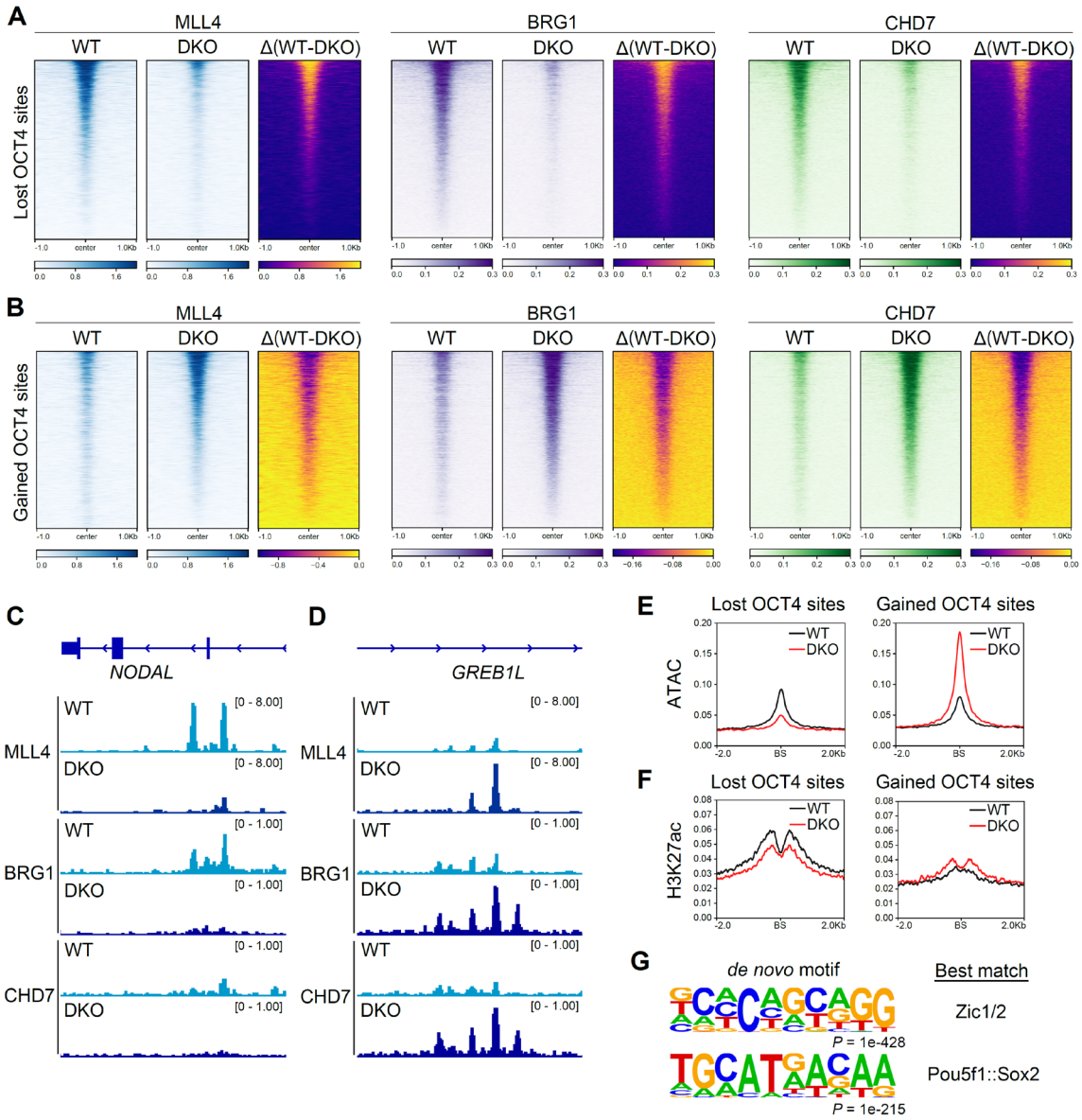

Figure 6. UTX and UTY are required for the distribution of chromatin remodeling factors
(A) Comparison of ChIP-seq signal intensities of chromatin remodeling factors between WT and DKO cells within a 2 kb region centered on OCT4 lost sites. (B) Comparison of ChIP-seq signal intensities of chromatin remodeling factors between WT and DKO cells within a 2 kb region centered on OCT4 gained sites. (C) Example of a region showing reduced binding of chromatin remodeling factors. (D) Example of a region showing increased binding of chromatin remodeling factors. (E) ATAC-seq signals at OCT4 relocation sites in WT and DKO cells. (F) H3K27ac ChIP-seq signals at OCT4 relocation sites in WT and DKO cells. (G) Enriched sequence motifs at OCT4 gained sites.

Akiyama_Fig.7

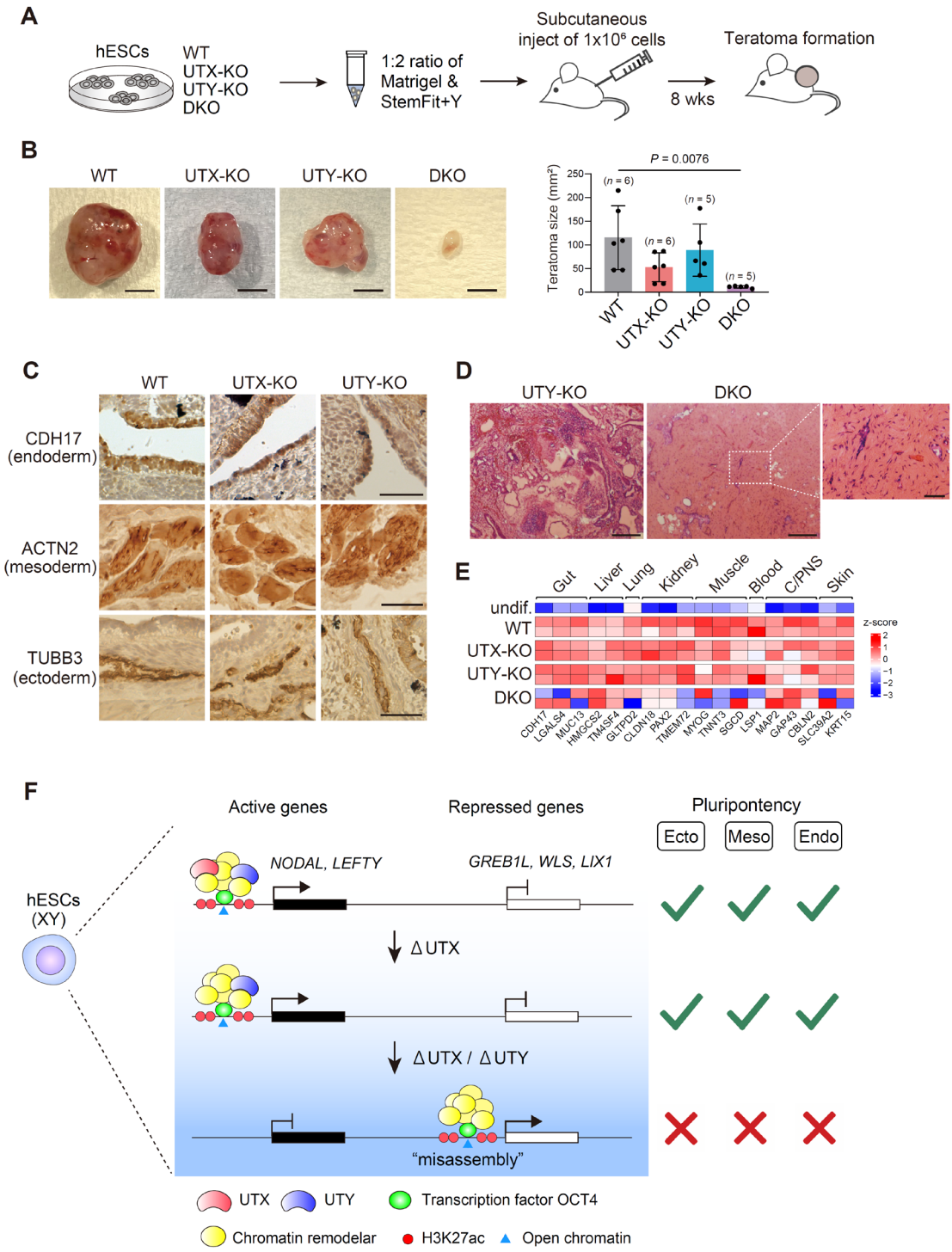

Figure 7. UTX and UTY are essential for sustaining pluripotency

(A) Schematic representation of the teratoma formation assay to assess pluripotency in vivo. (B) Representative images of teratomas derived from WT, UTX-KO, UTY-KO, and DKO ES cells. A graph showing the measurement of the teratoma sizes. Teratomas were not observed in DKO. (C) Immunohistochemical staining with the indicated antibodies on the teratoma sections showing the differentiation into the three germ layers in WT and single KO conditions. (D) Hematoxylin and eosin staining showing that tissue-like structures were rarely observed in the DKO-derived masses. (E) Expression of marker genes for each tissue type in the teratomas. (F) Schematic representation of the model illustrating UTY's role in facilitating transcription factor occupancy and maintaining pluripotency. In the absence of UTX, UTY is sufficient to preserve chromatin structure and maintain proper transcriptional regulation. However, when both UTX and UTY are absent, transcription factors and chromatin-associated complexes mislocalize—likely binding to alternative motifs—resulting in regulatory misassembly, ectopic activation of silent genes, and loss of pluripotency.